EDGE ARTICLE

Check for updates

A chiral fluorescent Ir(III) complex that targets the GPX4 and ErbB pathways to induce cellular ferroptosis†

Xinyang Zhao,‡[a] Jingyi Zhang,‡[a] Wei Zhang,[b] Zijian Guo, [a] Wei Wei,*[b] Xiuxiu Wang*[a] and Jing Zhao *[a]

Ferroptosis has recently emerged as a non-apoptotic form of programmed cell death and promising target for anticancer treatment. However, it is challenging to discover ferroptosis inducers with both highly selective tumour targeting and low cytotoxicity to normal cells. Here, we report an Ir(III) complex, **Ir1**, that contains a novel chiral pyridine RAS-selective lethal ligand (Py-RSL). This complex effectively inhibits glutathione peroxidase 4 (GPX4) and ferroptosis suppressor protein 1 (FSP1) to induce ferroptosis in human fibrosarcoma (HT-1080) cells. Notably, metal coordination not only endows **Ir1** with fluorescent properties for convenient cellular real-time tracking but also efficiently reduces the off-target toxicity of the Py-RSL ligand. Furthermore, label-free quantitative proteomic profiling revealed that **Ir1** simultaneously inhibits the ErbB signalling pathway to enhance tumour suppression. Our work is the first to report a ferroptosis-inducing iridium complex with dual mechanisms of inhibition and provides a highly selective and efficient route to develop new ferroptosis-inducing metallodrugs.

Introduction

Ferroptosis was first proposed in 2012 as an iron-dependent form of regulated cell death caused by unrestricted lipid peroxidation (LPO) and increased reactive oxygen species (ROS).[1–3] In the past decade, ferroptosis was shown to participate in neurodegenerative diseases,[4–6] cardiovascular diseases,[7] and especially cancer.[8,9] Ferroptosis plays important roles in the occurrence, development, and metastasis of tumours, suggesting its great potential in the development of antitumor treatments.[10–13] The reported ferroptosis inducers are mainly small organic molecules,[14,15] such as RAS-selective lethal 3 (RSL3)[16] and erastin (Scheme 1a).[17,18] However, their off-target toxicity and short half-life restrict their further application *in vivo* for clinical cancer treatment. Thus, developing ferroptosis inducers with both highly selective tumour targeting and low cytotoxicity to normal cells is still challenging.

In recent studies, various nanomaterials,[19–22] metal–organic frameworks (MOFs),[23–25] and metal complexes[26–32] have been reported to be effective in inducing ferroptosis. Metal complexes, especially transition metal complexes, have been widely used in bioimaging and cancer treatment for their good optical properties, great diversity of tunable ligands, and

[a]State Key Laboratory of Coordination Chemistry, Chemistry and Biomedicine Innovation Center (ChemBIC), School of Chemistry and Chemical Engineering, Nanjing University, Nanjing, 210023, China. E-mail: wangxiuxiu@nju.edu.cn; jingzhao@nju.edu.cn

[b]State Key Laboratory of Pharmaceutical Biotechnology, School of Life Sciences, Nanjing University, Nanjing, 210023, China. E-mail: weiwei@nju.edu.cn

† Electronic supplementary information (ESI) available. See DOI: https://doi.org/10.1039/d2sc06171f

‡ Equal contribution.

(a) Typical small-molecule ferroptosis inducers

RSL3

Erastin
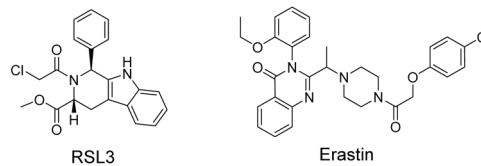
(b) Recent development of ferroptosis inducing metal complexes

R_1 = H, F,Cl, Br, CH_3, OCH_3, OCF_3, CH_3, NO_2
R_2 = H, CH_3

Ir(III)-Fe(II) bimetallic complex
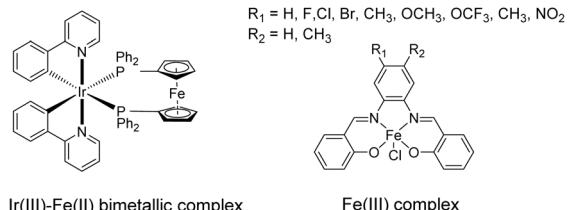
Fe(III) complex

(c) This work: rational design of Ir(III) complex targeting ferroptosis

Iridium hydrides + Py-RSL → Ir1

Scheme 1 Rational design of **Ir1**.
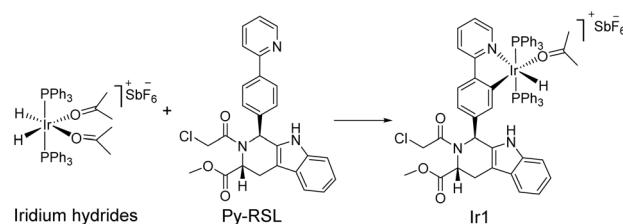
excellent targeting ability.[33–37] Specific to the metal coordination strategy, some significant breakthroughs have been made in the development of excellent metal complexes to induce ferroptosis. For example, Gust *et al.* pioneered a series of iron(III) complexes that generate lipid-based ROS and induce ferroptosis (Scheme 1b).[27,31] The significant breakthrough made by Mao *et al.* showed that a cyclometalated Ir(III) complex containing a ferrocene moiety ligand is a highly efficient ferroptosis inducer, providing a powerful tool for enhancing cancer immunity (Scheme 1b).[29] Chao *et al.* creatively designed a biodegradable Ir(III) coordination polymer that induces apoptosis and ferroptosis through photodynamic therapy.[30] Mechanistically, these current design strategies introduce exogenous iron into cells for its accumulation to perform the Fenton reaction or produce an overload of lipid peroxides to induce ferroptosis. Constructing an amide or ester bond or using existing coordination sites to conjugate natural products or drugs to metals have become common methods for metal drug design, which could increase the selectivity and reduce the side effects of the metal.[38,39] In addition, redesigning drug scaffolds as ligands while retaining the targeting group is an attractive strategy. Notably, reports on these strategies revealed that metal coordination could reduce toxicity and increase the pharmaceutical effect of the free drug molecules.[40] Through rational design, metal complexes can simultaneously combine the advantages of both metals and drug molecules to achieve better therapeutic effects.

It is noteworthy that iridium hydrides have been demonstrated to be effective scaffolds for metal drugs due to their adjustable photophysical and chemical properties.[41–44] Herein, we designed the iridium(III) complex **Ir1** based on iridium hydrides. To better target the glutathione peroxidase 4 (GPX4) protein, which is enriched in the mitochondria, we first introduced triphenylphosphine as the mitochondria-targeting ligand and then Py-RSL as the ferroptosis-inducing ligand (Scheme 1c). This complex induces ferroptosis in human fibrosarcoma (HT1080) cells by significantly inhibiting GPX4 and ferroptosis suppressor protein 1 (FSP1). Notably, intracellular localization monitoring can be achieved under visible light (488 nm) excitation. Moreover, iridium coordination reduces the toxicity of the Py-RSL ligand to make this complex available for *in vivo* applications.

Results and discussion

Synthesis of the Ir(III) complex Ir-Py-RSL

Six-coordinated hydrides of iridium provide an excellent starting point for a variety of modifications. The axial ligand triphenylphosphine gives additional mitochondrial targeting ability, while leaving coordination space in the plane for mono- or bidentate ligands. Among small molecule ferroptosis inducers, RSL3 has an ability to target GPX4,[45] and chloroacetamide is essential for its activity. Therefore, we preserved the pharmaceutical scaffold and replaced the phenyl at C1 with phenylpyridine for metal coordination (Fig. 1a). Four different chiral ligands (**L1–4**) and the four corresponding Ir(III) complexes (Ir-Py-RSL, **Ir1–4**) were then synthesized. [1]H two-
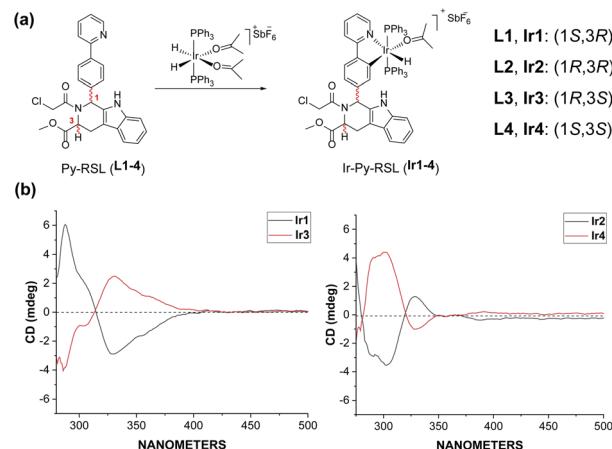
Fig. 1 (a) General synthetic route of Ir-Py-RSL. (b) CD spectra of **Ir1–4**.

dimensional nuclear Overhauser effect spectroscopy (NOESY) was performed to determine the identified stereochemistry of the four ligands. We also verified the chirality by circular dichroism (CD) spectra (Fig. 1b and S1†), and high-performance liquid chromatography (HPLC) was used to further prove the difference in ligand chirality (Fig. S2 and S3†). All Ir(III) complexes maintain stable at 37 °C after 48 hours (Fig. S4–S7†). We also assessed the octanol/water partition coefficients ($\log P_{O/W}$) of the complexes, which show similar lipophilicities (**Ir1**: 0.61 ± 0.22; **Ir2**: 0.64 ± 0.23; **Ir3**: 0.67 ± 0.12; **Ir4**: 0.54 ± 0.23). The details of the synthesis and characterization are fully described in ESI.†

Cytotoxicity of the iridium complexes

First, a cytotoxicity test in HT1080 cells was carried out by performing a CCK8 assay. As shown in Tables 1 and S1,† **L3** ($IC_{50} = 1.76$ μM) and **L1** ($IC_{50} = 1.71$ μM) displayed high cytotoxicity, whereas the IC_{50} values of **Ir3** and **Ir1** were 11.01 μM and 7.48 μM, respectively. Metal coordination reduces the toxicity of ligand by three- to fourfold. Notably, the other two chiral ligands and corresponding Ir(III) complexes did not show significant antitumor activity. Among them, **Ir1** showed antitumor toxicity superior to that of cisplatin ($IC_{50} = 9.72$ μM). We then chose human lung fibroblasts (HLFs) and human embryonic kidney 293T (HEK-293T) cells to determine the selectivity of the compounds against normal cells. As shown in Table 1, in

Table 1 IC_{50} value (μM) of the ligands and Ir(III) complexes[a]

Cell line	IC_{50} (μM)		
	L1	**Ir1**	Cisplatin
HT1080	1.71	7.48	9.72
PANC-1	1.45	9.19	21.33
HLF	1.44	46.76	10.82
HEK-293T	8.47	24.79	30.52

[a] Cell viability was measured by CCK8 assay after 48 h incubation with different complexes (dose–response curves are shown in Fig. S9).

comparison to **L1** and cisplatin, the Ir(III) complex showed much lower cytotoxicity towards HLFs, and the cytotoxicity to HEK-193T cells was comparable to that of cisplatin. The IC$_{50}$ values confirmed that Ir coordination not only reduced the toxicity of the ligand but also provided cancer cell selectivity. We confirmed these results in human pancreatic cancer (PANC-1) cells. The cellular uptake of **Ir1** was measured during 120 min (Fig. S10†). At the cellular level, compared with cisplatin, **Ir1** possessed better antitumor activity and fewer side effects in normal cells.

Ferroptosis induced by Ir1

Then, we verified the mode of cell death by concomitantly incubating the complexes with different inhibitors: ferrostatin-1 (Fer-1) and deferoxamine (DFO) for ferroptosis,[1] Z-VAD-FMK (Z-VAD) for apoptosis,[46] and necrostatin-1 (Nec-1) for necroptosis.[47] As displayed in Fig. 2a and S11,† none of the inhibitors showed clear influence on the ligand-mediated reduction in cell viability. For **Ir2**-treated cells, Z-VAD strongly restored cell viability, indicating that the complex caused apoptosis. **Ir4** induced ferroptosis as well as necroptosis, as confirmed by the enhanced cell viability after incubation with Fer-1 and Nec-1. In addition, the inhibitors showed no effect on **Ir3**-induced cell death. Notably, Fer-1 and DFO rescued **Ir1**-induced cell death, while the other inhibitors displayed no influence, indicating that ferroptotic cell death was induced by this complex (Fig. 2a).

Based on the above results, we further verified that ferroptosis was induced by **Ir1**. Glutathione depletion, GPX4 activity reduction, and decreased antioxidant capacity of cells resulting in increased lipid peroxidation reactions and reactive oxygen species (ROS), are common ferroptosis markers.[48,49] As shown in Fig. 2e and S12,† **Ir1** and the corresponding ligand both induced extensive ROS production. When compared with phosphate-buffered saline (PBS)- and **L1**-treated cells, **Ir1** caused notably increased lipid peroxidation (Fig. 2d and S12†). Additionally, Fer-1 could restore the cell viability of **L1**-treated cells. To analyse the causes of lipid ROS production, we detected the expression of two key targets, GPX4 and FSP1. GPX4 and FSP1 were significantly inhibited, which was confirmed by western blot and reverse transcription-polymerase chain reaction (RT-PCR) experiments (Fig. 2b and c). Above results suggested that **L1** acts as the ferroptosis-inducer, the replacement of C1 phenyl of RSL3 with phenylpyridine has no effect on the drug function. Another representative hallmark of ferroptosis is condensed mitochondrial morphology.[49] The transmission electron microscopy (TEM) image in Fig. 2f shows distinct, shrunken mitochondria and collapsed mitochondrial cristae. Altogether, as evidenced by the biochemical and morphological characteristics, these results further confirmed that ferroptosis was induced by **Ir1**. We also verified the death pattern by ferroptosis inhibitors, LPO and ROS production in a healthy cell line (HLF). The results indicate **Ir1** does not cause healthy cell to undergo ferroptosis (Fig. S13†).
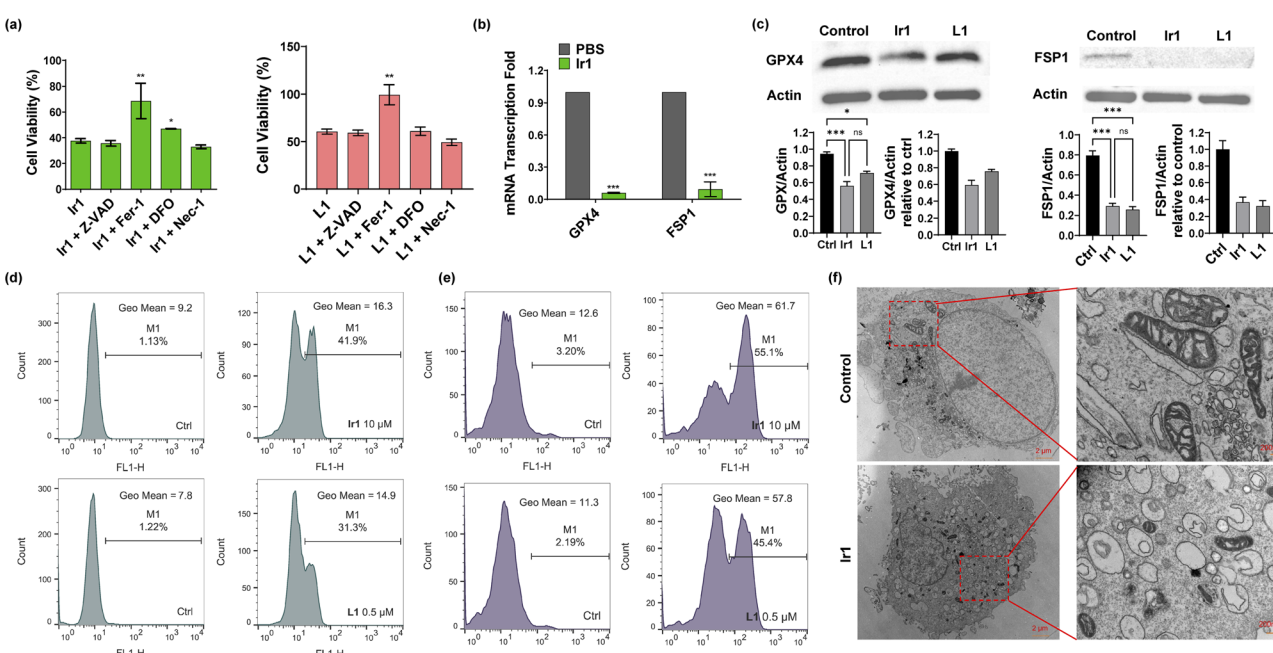
Fig. 2 Characterization of **Ir1**-induced ferroptosis. (a) Viability of HT1080 cells treated with 10 μM **Ir1**/0.5 μM **L1**, 10 μM **Ir1**/0.5 μM **L1** + 20 μM Z-VAD, 10 μM **Ir1**/0.5 μM **L1** + 2 μM Fer-1, 10 μM **Ir1**/0.5 μM **L1** + 40 μM DFO, and 10 μM **Ir1**/0.5 μM **L1** + 25 μM Nec-1 for 48 h. (b) Fold changes in GPX4 and FSP1 mRNA transcription in HT1080 cells treated with 10 μM **Ir1** and PBS as the control. (c) Expression of GPX4 and FSP1 in **Ir1**-, **L1**-, and PBS-treated HT1080 cells by western blot. (d) Lipid peroxidation in HT1080 cells treated with 0.5 μM **L1** and 10 μM **Ir1** with PBS as the control, determined by BODIPY-C11 staining *via* flow cytometry after 3 h incubation. (e) ROS production was evaluated by DCFH-DA staining after 3 h incubation in PBS-treated and 0.5 and 10 μM **L1**- and **Ir1**-treated HT1080 cells. (f) TEM images of control (PBS) and 10 μM **Ir1**-treated HT1080 cells after 24 h incubation; scale bars: 2 μm (left), 200 nm (right). Values are expressed as the mean ± SD ($n = 3$). Statistical significance was evaluated by *t* test or one-way ANOVA; ns $p \geq 0.05$, *$p < 0.05$, **$p < 0.01$, and ***$p < 0.001$.

Cellular imaging of Ir1

Under physiological conditions, metal complexes have better chemical and photochemical stability than organic molecules.[50,51] All Ir(III) complexes show ligand-based fluorescence at ≈575 nm with 488 nm excitation in dimethyl sulfoxide (Fig. 3a). Ultraviolet-visible spectra were also detected (Fig. S8†). Having excitation and emission wavelengths in the visible range could effectively avoid photodamage and photobleaching in cells, which is suitable for tracking action processes in cells. We made observations every ten minutes for two and a half hours. As illustrated in Fig. 3c and S14,† the Ir(III) complex gradually entered the cells from the extracellular space over 60 min and then acted on different organelles over time. To further localize the complex in organelles, we performed a colocalization assay at two time points with MitoTracker Red (MTR) for mitochondrial staining and 4′,6-diamidino-2-phenylindole (DAPI) for nuclear staining (Fig. 3d). At 90 min, the Ir(III) complex had aggregated and attached to cytoplasm, not in mitochondria, for the Pearson's correlation coefficient is only 0.0749. While at 150 min, some of the complexes had entered the nucleus while the rest remained mainly on the mitochondria (Pearson's correlation coefficient is 0.4734). The fluorescence images showed that the Ir(III) complex acted on the mitochondria to exert subsequent functions. We also quantified the iridium content in different organelles by inductively coupled plasma-

mass spectrometry (ICP-MS) after 24 h of treatment and found 67.7%, 13.2%, and 19.1% in the mitochondria, nucleus, and cytoplasm, respectively (Fig. 3b). The above results confirmed that Ir1 has good mitochondrial targeting ability. Notably, when the complex functions in specific organelles, a significant reduction in the off-target toxicity of the organic ligand can be achieved.

Proteomic analysis of Ir1

To further understand the mechanism of Ir1 in cells, we performed a label-free quantitative proteomic profiling experiment. This mass spectrometry-based technology provides new insights into cellular responses after metal complex exposure, including the interaction and regulation of cellular pathways, which can identify the altered pathways through extensive quantification of cellular proteins.[52–54] With advances in proteomic techniques, a deeper mechanistic understanding of cellular responses can be obtained, such as cellular uptake, biological distribution, and toxicity.[55–58] Fig. 4a and b show the significant differences in protein expression between the Ir1 group and PBS control group. It was found that 199 proteins were significantly downregulated and 280 proteins were upregulated in cells treated with Ir1 (Fig. 4c). Notably, eukaryotic translation initiation factor 2A (EIF2A), which plays a vital role in the integrated stress response of cancer cells, leading to drug resistance and poor prognosis, was the most inhibited protein.[59,60] The proteomics results also showed a large number of destroyed proteins (Table S2†), including GPX4, which was confirmed above. In addition, subcellular localization, Kyoto Encyclopedia of Genes and Genomes (KEGG) pathway annotation, and group domain enrichment analysis of the differentially expressed proteins including molecular function, cellular component, and protein domain are shown in Fig. S15–S19.†

Notably, Ir1 significantly affected ErbB signalling pathways, as revealed by bioinformatic analysis (Fig. 4d). The ErbB family is related to a variety of cancers, and its overexpression leads to cancer metastasis, drug resistance, poor prognosis, and a lower survival rate.[61,62] Targeting the ErbB family has thus become an effective means of cancer treatment.[63,64] Notably, ferroptosis is also considered to be an autophagy-dependent type of cell death, while ErbB-1 can mediate autophagy.[65] Additionally, autophagy could cause histone deacetylase inhibition, which promotes high mobility group box 1 (HMGB1) acetylation and leads to HMGB1 release in ferroptosis as a damage-associated molecular pattern molecule.[66] ErbB-1 inhibition was shown to contribute to ferroptosis.[67] Based on our proteomic data, we further verified the ErbB-targeting ability of Ir1 by qRT-PCR. We also detected the expression of a series of ErbB signalling pathway-related proteins. As shown in Fig. 4e, the expression of a disintegrin and metalloprotease 17 (ADAM17),[68] Huntingtin interacting protein 1 (HIP1),[69] Casitas B-lineage lymphoma (CBL),[70] nucleoporin 62 (NUP62),[71] short hairpin kinesin-binding protein (SHKBP),[72] docking protein 1 (DOK1),[73] and recombination signal binding protein (RBPJ)[74] was significantly suppressed. Coiled-coil domain containing 88 (CCD C88)[75] and
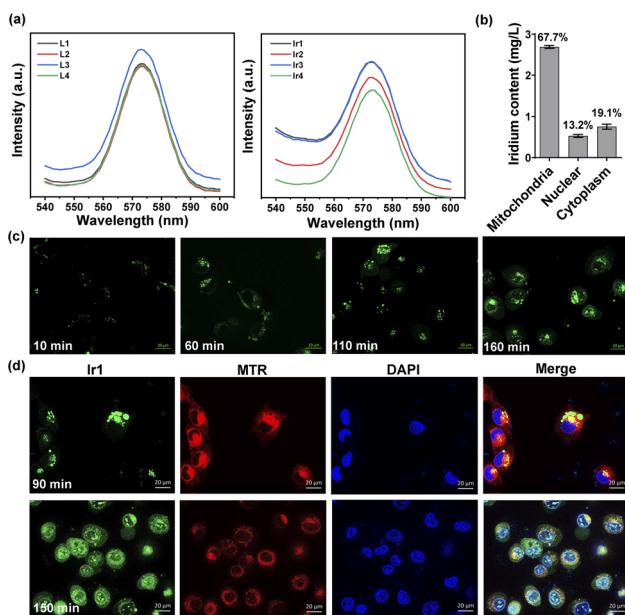
Fig. 3 Intracellular localization and organelle colocalization of Ir1 in treated HT1080 cells. (a) Fluorescence intensity of the four ligands and their corresponding Ir(III) complexes (10 μM in dimethyl sulfoxide) under 488 nm excitation. (b) Cellular distribution of iridium in HT1080 cells measured by quantitative ICP-MS after 12 h of incubation. (c) Microscopic images of HT1080 cells at different time points after incubation with 10 μM Ir1 ($\lambda_{ex/em}$ = 488/575 ± 20 nm); scale bar: 20 μm. (d) Microscopic images of HT1080 cells at 90 min and 150 min after Ir1 treatment, followed by incubation with 2 μM MTR ($\lambda_{ex/em}$ = 572/632 ± 10 nm) and 5 μM DAPI ($\lambda_{ex/em}$ = 375/488 ± 10 nm); scale bar: 20 μm.
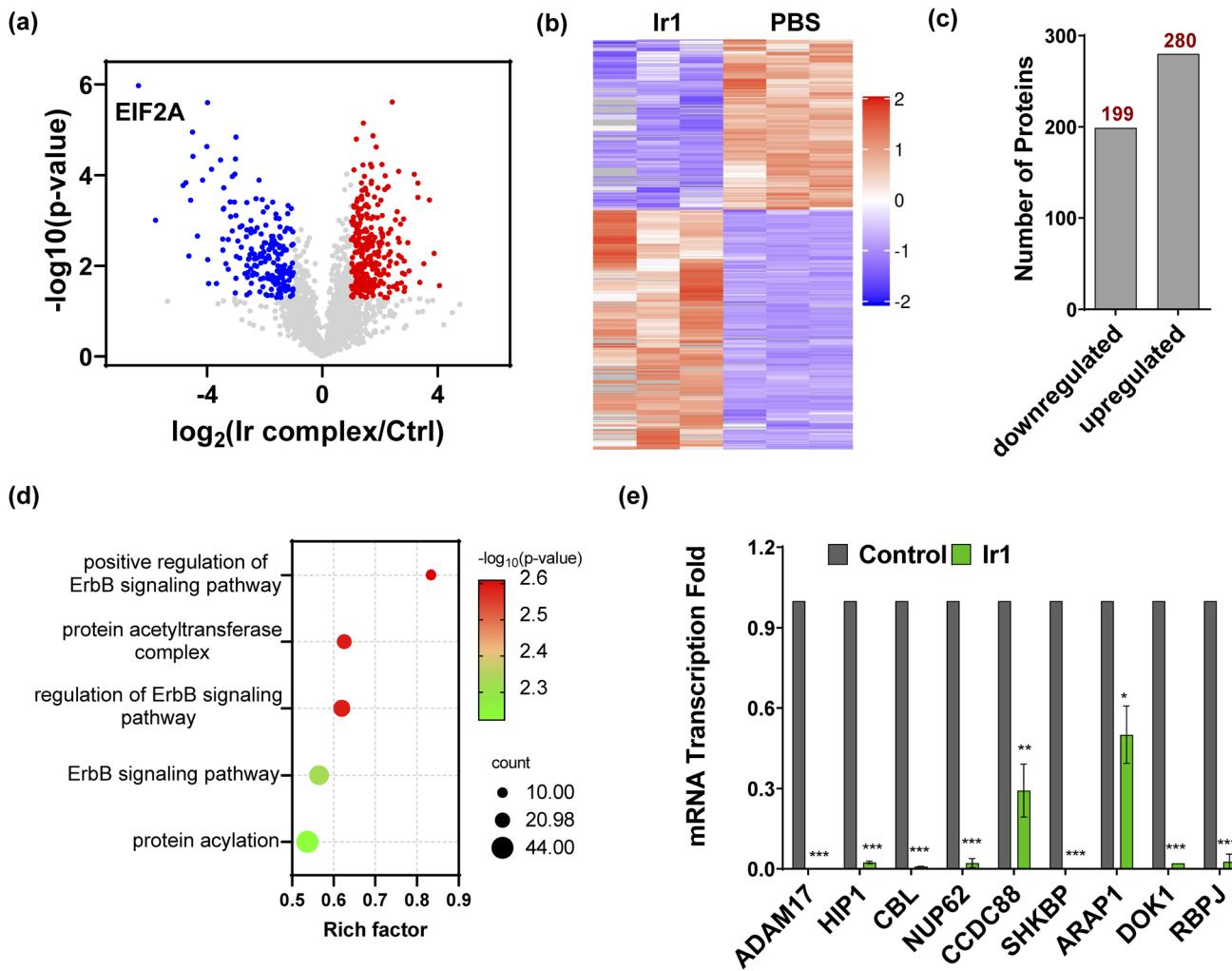
Fig. 4 Proteomics analysis of **Ir1**-treated cells compared with the control. (a) Volcano plot of downregulated proteins (blue), upregulated proteins (red), and unchanged proteins (grey). (b) Heatmap of the differentially expressed proteins (*$p < 0.05$). (c) The total number of down-regulated and upregulated proteins (*$p < 0.05$). (d) Bubble plot of the gene ontology analysis of ErbB pathway-related proteins. (e) mRNA transcription fold changes in ADAM17, HIP1, CBL, NUP62, CCDC88, SHKBP, ARAP1, DOK1, and RBPJ in HT1080 cells treated with 10 μM **Ir1** and PBS as the control. Values are expressed as the mean ± SD ($n = 3$). Statistical significance was evaluated by t test; *$p < 0.05$, **$p < 0.01$, and ***$p < 0.001$.

angiotensin II type 1 receptor-associated protein (ARAP1)[76] were also inhibited to varying degrees. These results verified that **Ir1** could inhibit the ErbB signalling pathway, which could further enhance anticancer activity and contribute to ferroptosis. Such dual-targeting abilities makes this Ir(III) complex a promising agent for future anticancer applications *in vivo*.

Toxicity of Ir1 *in vivo*

To further apply the **Ir1** complex *in vivo*, we first detected its toxicity in mice to evaluate its safety. Blood biochemical and haematological analyses were performed 7 days after injection of **Ir1**, with **L1** and PBS used for comparison. For blood biochemical tests, the indices of aspartate transaminase (AST), alanine transaminase (ALT), and blood urea nitrogen (BUN) are shown in Fig. 5a. Compared with PBS-treated mice, the ALT values significantly increased in **Ir1**- and **L1**-treated group, and

only **L1** induced a significant increase in the AST levels. **L1**-induced raise in ALT and AST level are extremely significant compared to **Ir1** treatment. These results indicate **L1** causes more damage to the hepatocyte organelles. Higher level of UREA caused by **L1** also shows that there is a certain kidney damage. From the haematological analysis, the values of white blood cells (WBCs), red blood cells (RBCs), haemoglobin (HGB), and platelets (PLTs) showed no statistical difference between **Ir1** and control group (Fig. 5b). But the RBC, HGB, and PLT levels of **L1** all have a statistically significant decrease compared to the control group. **Ir1** is therefore safer than **L1** *in vivo* according to the above indices. Furthermore, there were no significant effects on the body weight among each group (Fig. 5c). These results indicated that **Ir1** does not trigger hepatic or kidney toxicity, while **L1** could cause severe liver damage, which further illustrates the detoxification ability of Ir(III) coordination.
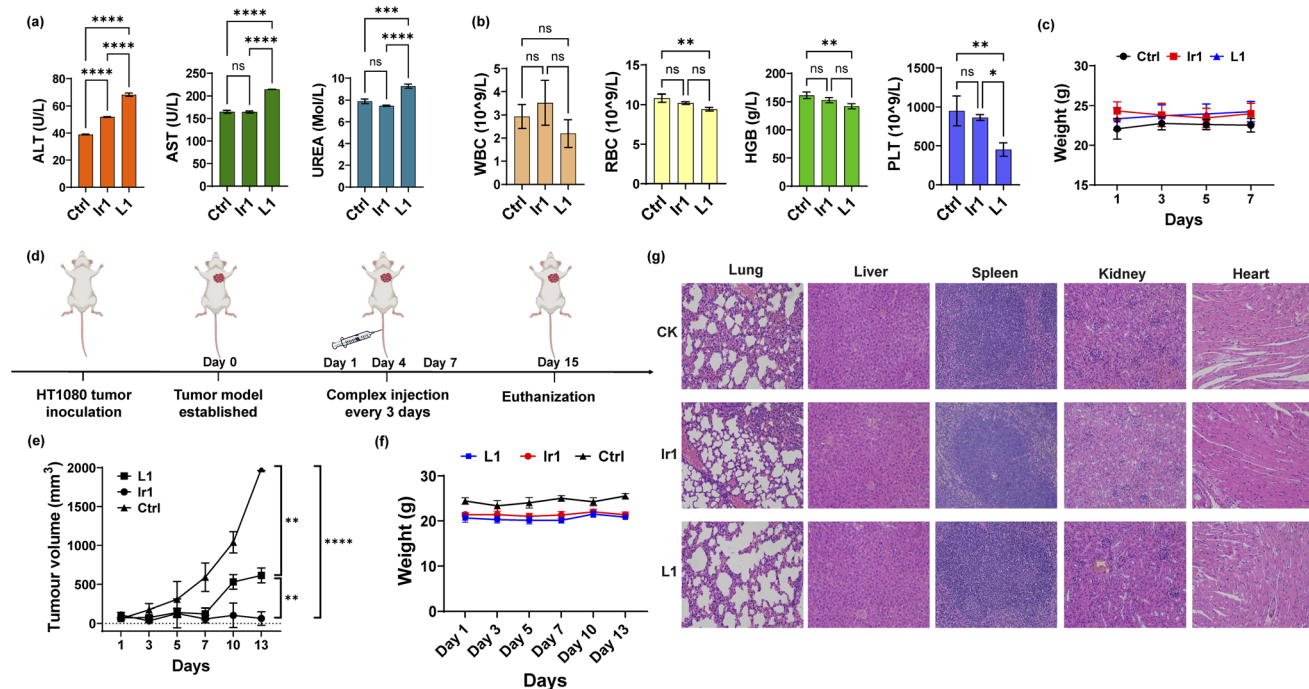
Fig. 5 *In vivo* toxicity and antitumor tests. (a) Biochemical analysis (ALT, AST, and UREA) and (b) haematological analysis (RBCs, WBCs, HGB, and PLT) of the blood from mice 7 days postinjection with **Ir1** (5 mg kg^{-1}), **L1** (5 mg kg^{-1}), and PBS. (c) The body weights of the mice injected with the respective compounds over 7 days. (d) Schematic diagram of the *in vivo* experiment. (e) The tumour volume curves and (f) mouse body weight over 13 days. (g) Haematoxylin and eosin (H&E) staining of the liver, spleen, kidney, heart, and lung tissues of the mice at 7 days postinjection. Image magnification: 200×. Values are expressed as the mean $\pm$ SD ($n = 3$). Statistical significance was evaluated by *t* test or one-way ANOVA; ns $p \geq 0.05$, *$p < 0.05$, **$p < 0.01$, ***$p < 0.001$, and ****$p < 0.0001$.

Antitumor activity of Ir1 in mice

Finally, we conducted antitumor experiments in mice. HT-1080 cells were first implanted into three groups of mice. After the tumour-bearing mouse model was constructed, **Ir1** (5 mg kg^{-1}), **L1** (5 mg kg^{-1}), and PBS were injected through the tail vein on Days 1, 4, and 7 (Fig. 5d). Tumour volumes and mouse body weights were recorded for 15 days. As shown in Fig. 5e, compared with PBS group, the **Ir1** and the **L1** treatment could both inhibit tumour volume, and the **Ir1** group exhibited greater tumour suppression. This is probably due to the tumour-targeting ability of the iridium complex, a property that the off-targeted ligand molecule lacks. *t* test results also showed
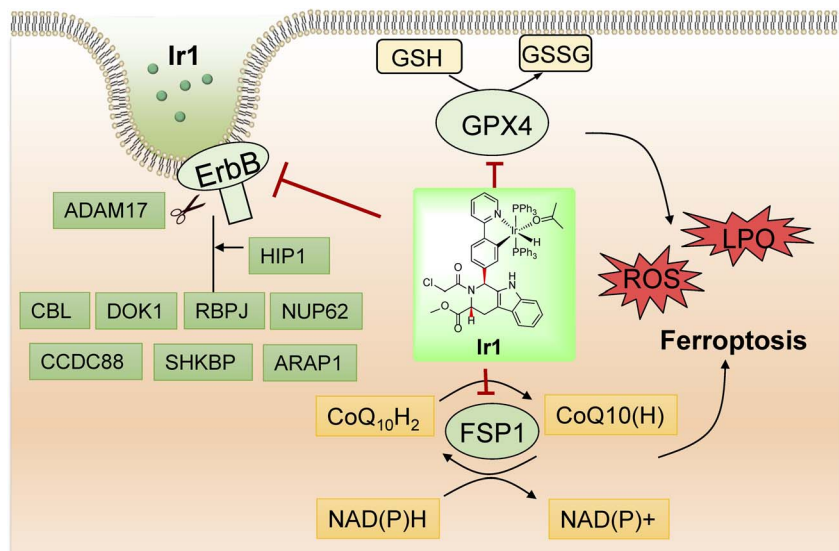
Fig. 6 Schematic illustration of the biological mechanism of **Ir1** in cancer cells based on the experiment results and proteomic analysis of **Ir1**.

a significant difference between these two treatments ($p < 0.0001$). Additionally, there was no clear loss in mouse body weight in any of the groups (Fig. 5f). All mice were sacrificed after 15 days for organ slicing. Haematoxylin and eosin (H&E) staining showed that the Ir(III) complex did not cause toxic damage to any organ, while the ligand damaged the lung and kidney (Fig. 5g). Although **L1** is more toxic *in vitro*, **Ir1** showed better antitumor ability *in vivo*. The iridium complex provided better targeting capabilities, and the dual-targeting effect makes **Ir1** a promising anticancer agent for future cancer treatment.

Conclusions

In summary, we synthesized a novel iridium complex, **Ir1**, which contains a Py-RSL ligand, and found that this complex could induce ferroptosis and overcome the disadvantages of small organic molecules. In detail, **Ir1** induced ferroptosis in cancer cells by inhibiting the critical proteins GPX4 and FSP1 (Fig. 6). *In vitro* and *in vivo* experiments demonstrated that metal coordination could reduce the off-target toxicity of the Py-RSL ligand *in vivo*, and visible light-excited fluorescence enabled real-time imaging to determine compound localization *in vitro*. Notably, the ErbB signalling pathway was also inhibited by **Ir1**, which further contributed to its anticancer activity and ferroptosis induction, making the complex more suitable for cancer treatment. Here, we introduced a dual-targeting ferroptosis inducer through rational design, which provides new insights into the design of multifunctional anticancer complexes.

Ethical statement

All animal studies were performed in accordance with the Guidelines for the Care and Use of Laboratory Animals of the Chinese Animal Welfare Committee and approved by The Institutional Animal Care and Use Committee (Nanjing University, IACUC-2109009).

Data availability

The data that support the findings of this study are available in the ESI† or on request from the corresponding author.

Author contributions

Prof. Zi-Jian Guo and Prof. Jing Zhao conceived and designed the study. Xin-Yang Zhao carried out the synthesis. Xin-Yang Zhao, Jing-Yi Zhang, Wei Zhang, and Xiu-Xiu Wang performed the *in vitro* and *in vivo* experiments. Xin-Yang Zhao, Xiu-Xiu Wang, Prof. Wei Wei, Prof. Jing Zhao, and Prof. Zi-Jian Guo wrote the manuscript. All authors reviewed, provided suggestions, and approved the final version. Xin-Yang Zhao and Xiu-Xiu Wang contributed equally.

Conflicts of interest

There are no conflicts to declare.

Acknowledgements

Notes and references

1 S. J. Dixon, K. M. Lemberg, M. R. Lamprecht, R. Skouta, E. M. Zaitsev, C. E. Gleason, D. N. Patel, A. J. Bauer, A. M. Cantley, W. S. Yang, B. Morrison and B. R. Stockwell, *Cell*, 2012, **149**, 1060–1072.

2 X. Jiang, B. R. Stockwell and M. Conrad, *Nat. Rev. Mol. Cell Biol.*, 2021, **22**, 266–282.

3 B. R. Stockwell, J. P. Friedmann Angeli, H. Bayir, A. I. Bush, M. Conrad, S. J. Dixon, S. Fulda, S. Gascón, S. K. Hatzios, V. E. Kagan, K. Noel, X. Jiang, A. Linkermann, M. E. Murphy, M. Overholtzer, A. Oyagi, G. C. Pagnussat, J. Park, Q. Ran, C. S. Rosenfeld, K. Salnikow, D. Tang, F. M. Torti, S. V. Torti, S. Toyokuni, K. A. Woerpel and D. D. Zhang, *Cell*, 2017, **171**, 273–285.

4 B. Do Van, F. Gouel, A. Jonneaux, K. Timmerman, P. Gelé, M. Pétrault, M. Bastide, C. Laloux, C. Moreau, R. Bordet, D. Devos and J.-C. Devedjian, *Neurobiol. Dis.*, 2016, **94**, 169–178.

5 R.-P. Zhou, Y. Chen, X. Wei, B. Yu, Z.-G. Xiong, C. Lu and W. Hu, *Theranostics*, 2020, **10**, 11976–11997.

6 T. Zhao, X. Guo and Y. Sun, *Aging Dis.*, 2021, **12**, 529–551.

7 J. Ju, Y.-n. Song and K. Wang, *Aging Dis.*, 2021, **12**, 261–276.

8 B. Hassannia, P. Vandenabeele and T. Vanden Berghe, *Cancer Cell*, 2019, **35**, 830–849.

9 X. Chen, R. Kang, G. Kroemer and D. Tang, *Nat. Rev. Clin. Oncol.*, 2021, **18**, 280–296.

10 J. Li, F. Cao, H.-l. Yin, Z.-j. Huang, Z.-t. Lin, N. Mao, B. Sun and G. Wang, *Cell Death Dis.*, 2020, **11**, 88.

11 C. M. Bebber, F. Müller, L. Prieto Clemente, J. Weber and S. von Karstedt, *Cancers*, 2020, **12**, 164.

12 J. P. Friedmann Angeli, D. V. Krysko and M. Conrad, *Nat. Rev. Cancer*, 2019, **19**, 405–414.

13 Z. Shen, J. Song, B. C. Yung, Z. Zhou, A. Wu and X. Chen, *Adv. Mater.*, 2018, **30**, 1704007.

14 G. Greco, E. Catanzaro and C. Fimognari, *Cancers*, 2021, **13**, 304.

15 C. Liang, X. Zhang, M. Yang and X. Dong, *Adv. Mater.*, 2019, **31**, 1904197.

16 W. S. Yang, R. SriRamaratnam, M. E. Welsch, K. Shimada, R. Skouta, V. S. Viswanathan, J. H. Cheah, P. A. Clemons, A. F. Shamji, C. B. Clish, L. M. Brown, A. W. Girotti, V. W. Cornish, S. L. Schreiber and B. R. Stockwell, *Cell*, 2014, **156**, 317–331.

17 S. Dolma, S. L. Lessnick, W. C. Hahn and B. R. Stockwell, *Cancer Cell*, 2003, **3**, 285–296.

18 M. Sato, R. Kusumi, S. Hamashima, S. Kobayashi, S. Sasaki, Y. Komiyama, T. Izumikawa, M. Conrad, S. Bannai and H. Sato, *Sci. Rep.*, 2018, **8**, 968.

19 S. Xu, H. Zheng, R. Ma, D. Wu, Y. Pan, C. Yin, M. Gao, W. Wang, W. Lì, S. Liu, Z. Chai and R. Li, *Nat. Commun.*, 2020, **11**, 3484.

20 H. Zheng, J. Jiang, S. Xu, W. Liu, Q. Xie, X. Cai, J. Zhang, S. Liu and R. Li, *Nanoscale*, 2021, **13**, 2266–2285.

21 L. Luo, H. Wang, W. Tian, X. Li, Z. Zhu, R. Huang and H. Luo, *Theranostics*, 2021, **11**, 9937–9952.

22 H. Liang, X. Wu, G. Zhao, K. Feng, K. Ni and X. Sun, *J. Am. Chem. Soc.*, 2021, **143**, 15812–15823.

23 E. Ploetz, A. Zimpel, V. Cauda, D. Bauer, D. C. Lamb, C. Haisch, S. Zahler, A. M. Vollmar, S. Wuttke and H. Engelke, *Adv. Mater.*, 2020, **32**, 1907267.

24 X. Meng, J. Deng, F. Liu, T. Guo, M. Liu, P. Dai, A. Fan, Z. Wang and Y. Zhao, *Nano Lett.*, 2019, **19**, 7866–7876.

25 H. He, L. Du, H. Guo, Y. An, L. Lu, Y. Chen, Y. Wang, H. Zhong, J. Shen, J. Wu and X. Shuai, *Small*, 2020, **16**, 2001251.

26 X. Wang, F. Chen, J. Zhang, J. Sun, X. Zhao, Y. Zhu, W. Wei, J. Zhao and Z. Guo, *Sci. China: Chem.*, 2020, **63**, 65–72.

27 J. Sagasser, B. N. Ma, D. Baecker, S. Salcher, M. Hermann, J. Lamprecht, S. Angerer, P. Obexer, B. Kircher and R. Gust, *J. Med. Chem.*, 2019, **62**, 8053–8061.

28 H. Yuan, Z. Han, Y. Chen, F. Qi, H. Fang, Z. Guo, S. Zhang and W. He, *Angew. Chem., Int. Ed.*, 2021, **60**, 8174–8181.

29 W.-J. Wang, Y.-Y. Ling, Y.-M. Zhong, Z.-Y. Li, C.-P. Tan and Z.-W. Mao, *Angew. Chem., Int. Ed.*, 2022, **61**, e202115247.

30 L. Ke, F. Wei, L. Xie, J. Karges, Y. Chen, L. Ji and H. Chao, *Angew. Chem., Int. Ed.*, 2022, e202205429.

31 D. Baecker, Ö. Sesli, L. Knabl, S. Huber, D. Orth-Höller and R. Gust, *Eur. J. Med. Chem.*, 2021, **209**, 112907.

32 M. Hreusova, V. Novohradsky, L. Markova, H. Kostrhunova, I. Potočňák, V. Brabec and J. Kasparkova, *Bioinorg. Chem. Appl.*, 2022, **2022**, 3095749.

33 E. J. Anthony, E. M. Bolitho, H. E. Bridgewater, O. W. L. Carter, J. M. Donnelly, C. Imberti, E. C. Lant, F. Lermyte, R. J. Needham, M. Palau, P. J. Sadler, H. Shi, F.-X. Wang, W.-Y. Zhang and Z. Zhang, *Chem. Sci.*, 2020, **11**, 12888–12917.

34 N. P. E. Barry and P. J. Sadler, *Chem. Commun.*, 2013, **49**, 5106–5131.

35 A. Casini, A. Vessières and S. M. Meier-Menches, *Metal-based anticancer agents*, Royal Society of Chemistry, 2019.

36 X. Wang and Z. Guo, *Chem. Soc. Rev.*, 2013, **42**, 202–224.

37 L. Zeng, P. Gupta, Y. Chen, E. Wang, L. Ji, H. Chao and Z.-S. Chen, *Chem. Soc. Rev.*, 2017, **46**, 5771–5804.

38 D.-L. Ma, C. Wu, S.-S. Cheng, F.-W. Lee, Q.-B. Han and C.-H. Leung, *Int. J. Mol. Sci.*, 2019, **20**, 341.

39 L. B. Heras, Á. Amesty, A. Estévez-Braun and S. Hortelano, *Anti-Cancer Agents Med. Chem.*, 2019, **19**, 48–65.

40 S. Pattan, S. Pawar, S. Vetal, U. Gharate and S. Bhawar, *Indian Drugs*, 2012, **49**, 5–12.

41 X. Song, Y. Qian, R. Ben, X. Lu, H.-L. Zhu, H. Chao and J. Zhao, *J. Med. Chem.*, 2013, **56**, 6531–6535.

42 X. Wang, M. Zhu, F. Gao, W. Wei, Y. Qian, H.-K. Liu and J. Zhao, *J. Inorg. Biochem.*, 2018, **180**, 179–185.

43 X. Wang, J. Zhang, X. Zhao, W. Wei and J. Zhao, *Metallomics*, 2019, **11**, 1344–1352.

44 S. Roy, M. Mohanty, R. G. Miller, S. A. Patra, S. Lima, A. Banerjee, N. Metzler-Nolte, E. Sinn, W. Kaminsky and R. Dinda, *Inorg. Chem.*, 2020, **59**, 15526–15540.

45 T.-J. Park, J. H. Park, G. S. Lee, J.-Y. Lee, J. H. Shin, M. W. Kim, Y. S. Kim, J.-Y. Kim, K.-J. Oh, B.-S. Han, W.-K. Kim, Y. Ahn, J. H. Moon, J. Song, K.-H. Bae, D. H. Kim, E.-W. Lee and S. C. Lee, *Cell Death Dis.*, 2019, **10**, 835.

46 E. A. Slee, H. Zhu, S. C. Chow, M. MacFarlane, D. W. Nicholson and G. M. Cohen, *Biochem. J.*, 1996, **315**, 21–24.

47 A. Degterev, Z. Huang, M. Boyce, Y. Li, P. Jagtap, N. Mizushima, G. D. Cuny, T. J. Mitchison, M. A. Moskowitz and J. Yuan, *Nat. Chem. Biol.*, 2005, **1**, 112–119.

48 Y. Xie, W. Hou, X. Song, Y. Yu, J. Huang, X. Sun, R. Kang and D. Tang, *Cell Death Differ.*, 2016, **23**, 369–379.

49 J. Y. Cao and S. J. Dixon, *Cell. Mol. Life Sci.*, 2016, **73**, 2195–2209.

50 Q. Zhao, C. Huang and F. Li, *Chem. Soc. Rev.*, 2011, **40**, 2508–2524.

51 R. J. Mortimer and N. M. Rowley, in *Comprehensive Coordination Chemistry II*, ed. J. A. McCleverty and T. J. Meyer, Pergamon, Oxford, 2003, pp. 581–619.

52 X. Wang, Y. Hu, J. Mo, J. Zhang, Z. Wang, W. Wei, H. Li, Y. Xu, J. Ma, J. Zhao, Z. Jin and Z. Guo, *Angew. Chem., Int. Ed.*, 2020, **59**, 5151–5158.

53 T. Verano-Braga, R. Miethling-Graff, K. Wojdyla, A. Rogowska-Wrzesinska, J. R. Brewer, H. Erdmann and F. Kjeldsen, *ACS Nano*, 2014, **8**, 2161–2175.

54 S. Gioria, H. Chassaigne, D. Carpi, A. Parracino, S. Meschini, P. Barboro and F. Rossi, *Toxicol. Lett.*, 2014, **228**, 111–126.

55 L. M. Wang, J. Y. Li, J. Pan, X. M. Jiang, Y. L. Ji, Y. F. Li, Y. Qu, Y. L. Zhao, X. C. Wu and C. Y. Chen, *J. Am. Chem. Soc.*, 2013, **135**, 17359–17368.

56 R. Cai and C. Y. Chen, *Adv. Mater.*, 2019, **31**, 1805740.

57 M. J. Cao, R. Cai, L. N. Zhao, M. Y. Guo, L. M. Wang, Y. C. Wang, L. L. Zhang, X. F. Wang, H. D. Yao, C. Y. Xie, Y. L. Cong, Y. Guan, X. Y. Tao, Y. L. Wang, S. X. Xu, Y. Liu, Y. L. Zhao and C. Y. Chen, *Nat. Nanotechnol.*, 2021, **16**, 708–716.

58 M. Y. Guo, L. N. Zhao, J. Liu, X. F. Wang, H. D. Yao, X. L. Chang, Y. Liu, J. M. Liu, M. You, J. Y. Ren, F. H. Wang, L. M. Wang, Y. L. Wang, H. B. A. Liu, Y. L. Li, Y. L. Zhao, R. Cai and C. Y. Chen, *Nano Lett.*, 2021, **21**, 6005–6013.

59 L. Chen, J. He, J. Zhou, Z. Xiao, N. Ding, Y. Duan, W. Li and L.-Q. Sun, *J. Cell. Mol. Med.*, 2019, **23**, 6060–6071.

60 A. A. Komar and W. C. Merrick, *Int. J. Mol. Sci.*, 2020, **21**, 2054.

61 C. L. Arteaga and J. A. Engelman, *Cancer Cell*, 2014, **25**, 282–303.

62 N. E. Hynes and H. A. Lane, *Nat. Rev. Cancer*, 2005, **5**, 341–354.

63 Y. Yarden and G. Pines, *Nat. Rev. Cancer*, 2012, **12**, 553–563.

64 N. Tebbutt, M. W. Pedersen and T. G. Johns, *Nat. Rev. Cancer*, 2013, **13**, 663–673.

65 B. Zhou, J. Liu, R. Kang, D. J. Klionsky, G. Kroemer and D. Tang, *Semin. Cancer Biol.*, 2020, **66**, 89–100.

66 Q. Wen, J. Liu, R. Kang, B. Zhou and D. Tang, *Biochem. Biophys. Res. Commun.*, 2019, **510**, 278–283.

67 X. Wu, H. Sheng, L. Zhao, M. Jiang, H. Lou, Y. Miao, N. Cheng, W. Zhang, D. Ding and W. Li, *Cell Death Dis.*, 2022, **13**, 557.

68 C. P. Blobel, *Nat. Rev. Mol. Cell Biol.*, 2005, **6**, 32–43.

69 D. S. Rao, S. V. Bradley, P. D. Kumar, T. S. Hyun, D. Saint-Dic, K. Oravecz-Wilson, C. G. Kleer and T. S. Ross, *Cancer Cell*, 2003, **3**, 471–482.

70 L. M. Grøvdal, E. Stang, A. Sorkin and I. H. Madshus, *Exp. Cell Res.*, 2004, **300**, 388–395.

71 Y. Leng, C. Cao, J. Ren, L. Huang, D. Chen, M. Ito and D. Kufe, *J. Biol. Chem.*, 2007, **282**, 19321–19330.

72 L. Feng, J.-T. Wang, H. Jin, K. Qian and J.-G. Geng, *Cell Biochem. Funct.*, 2011, **29**, 589–596.

73 J.-G. Némorin and P. Duplay, *J. Biol. Chem.*, 2000, **275**, 14590–14597.

74 Y. Chen, W. H. Fischer and G. N. Gill, *J. Biol. Chem.*, 1997, **272**, 14110–14114.

75 P. Ghosh, A. O. Beas, S. J. Bornheimer, M. Garcia-Marcos, E. P. Forry, C. Johannson, J. Ear, B. H. Jung, B. Cabrera, J. M. Carethers and M. G. Farquhar, *Mol. Biol. Cell*, 2010, **21**, 2338–2354.

76 T. Daniele, G. Di Tullio, M. Santoro, G. Turacchio and M. A. De Matteis, *Traffic*, 2008, **9**, 2221–2235.